Tenth International Conference on Computational Fluid Dynamics (ICCFD10), Barcelona,Spain, July 9-13, 2018 **ICCFD10-2018-0015**

A New Mapped WENO Method for Hyperbolic Problems

U S Vevek*, Zang B.* and New T.H.*
Corresponding author: dthnew@ntu.edu.sg

* Nanyang Technological University, Singapore.

Abstract: In this study, a new family of rational mapping functions $g_{\mathrm{RM}}(\omega; k,\ m,\ s)$ is introduced for seventh order WENO schemes. g_{RM} is a more general family of mapping functions which includes other mapping functions such as g_{M} [1] and g_{IM} [2] as special cases. The mapped WENO scheme WENO-IM(2,0.1) which uses $g_{\mathrm{IM}}(\omega;\ 2,\ 0.1)$ performs excellently at fifth order but rather poorly at seventh order. The reason for this loss of accuracy was found to be the over-amplification of very small weights by the mapping process which can be traced back to the large slope of $g_{\mathrm{IM}}(\omega;\ 2,\ 0.1)$ at $\omega = 0$. For $m > 1$, g_{RM} can be designed to have unit slope at $\omega = 0$ which will preserve small weights with little to no amplification. It has been demonstrated through several linear advection test cases that the mapped WENO scheme WENO-RM(4,4,40) which uses the mapping function $g_{\mathrm{RM}}(\omega; 4,\ 4,\ 20)$ outperforms both WENO-M and WENO-IM(2,0.1) at seventh order.

Keywords: Hyperbolic Problems, Finite Volume, High Order, Mapped WENO.

1 Introduction

Hyperbolic problems arise in many scientific and engineering applications. The Euler equations governing the dynamics of an inviscid fluid is a notable example of a non-linear hyperbolic problem. Hyperbolic problems admit discontinuities to develop and persist in the solutions. Needless to say, it is imperative to capture these discontinuities accurately. Conventional high order schemes, which perform excellently in the smooth regions of the solution, tend to produce spurious oscillations in the vicinity of discontinuities. Essentially non-oscillatory (ENO) schemes [3] were designed to overcome this problem by choosing the smoothest stencil to reconstruct the solution, thereby, effectively avoiding reconstruction across a discontinuity. Later, Liu, et al. [4] proposed the weighted ENO (WENO) scheme in which a weighted reconstruction is obtained from all available stencils. The weight assigned to each stencil was inversely proportional to the smoothness of the reconstruction within that stencil. In addition to remaining (essentially) non-oscillatory near discontinuities, the WENO method was able to attain $(r+1)^{th}$ order of convergence in smooth regions - one order higher than the approximations from the constituent stencils each of which converge at only r^{th} order. Jiang and Shu [5] improved upon the WENO scheme by proposing a new smoothness indicator which allowed the WENO method to achieve the optimal $(2r-1)^{th}$ order of convergence in smooth regions. This improved scheme is commonly referred to as WENO-JS.

The WENO-JS method has since become a popular choice for solving hyperbolic problems numerically due to its robustness and accuracy. However, a crucial detail remained unnoticed for several years until the work of Henrick, et al. [1]. They showed that the fifth order WENO-JS scheme fails to achieve the optimal fifth order convergence near critical points in the solution where the first derivative of the solution vanished. They explained that the loss of accuracy was masked when a relatively large value such as 10^{-6} used for ϵ, a parameter that was thought to be inconsequential and introduced solely to prevent division by zero (see Eq.(10)). In addition, they proposed a mapping function g_{M} to modify the WENO-JS stencil weights to recover the optimal order of accuracy near critical points. This scheme is referred to as WENO-M. More recently, it was shown that g_{M} actually belongs to a more general family of functions g_{IM} [2]. Using a different set of parameters, Feng, et al. [2] showed that vastly superior results could be obtained for

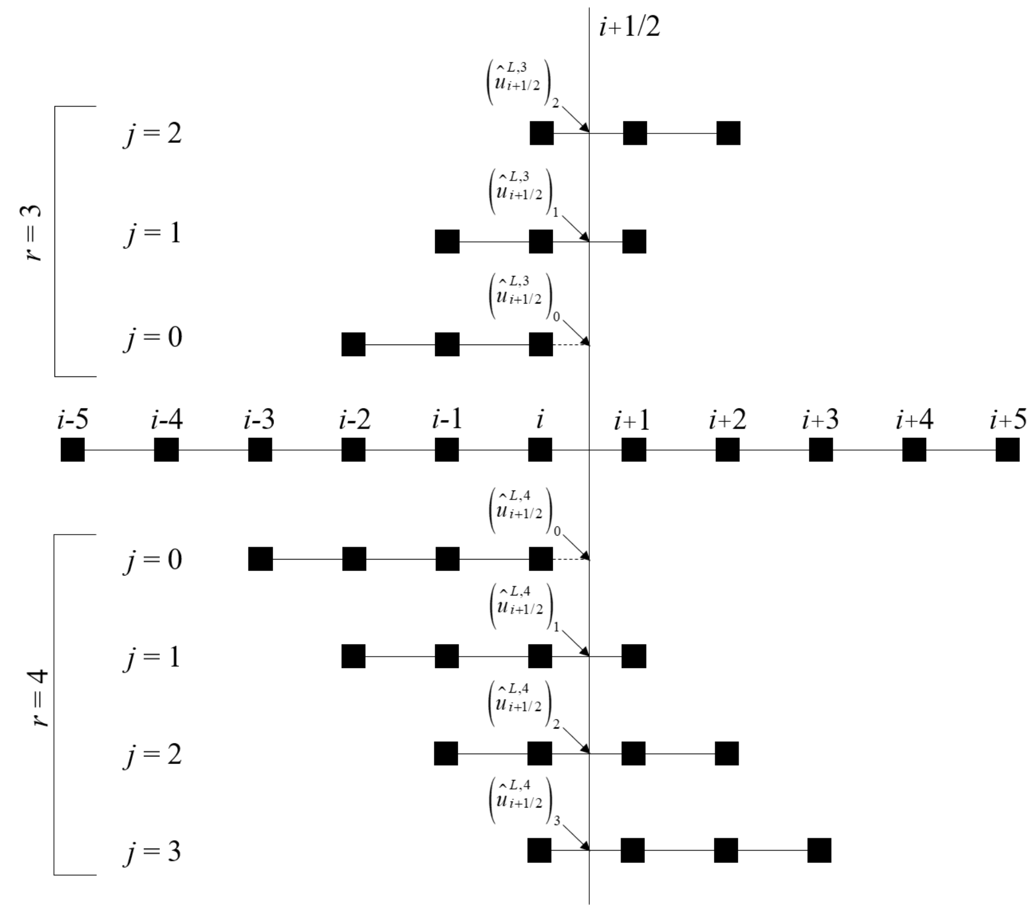

Figure 1: Schematic of stencils for fifth ($r = 3$) and seventh ($r = 4$) order WENO reconstructions.

fifth order WENO. Interestingly, this improved scheme, referred to WENO-IM(2,0.1), was able to capture discontinuities with very little dissipation compared to WENO-M and WENO-JS. However, when applied to seventh order WENO scheme, it was reported to be perform poorly.

In this study, the performances of the mapped methods are analyzed for fifth and seventh order WENO schemes. In particular, the cause behind the poor performance of WENO-IM(2,0.1) at seventh order is studied in detail. Based on the insights gleaned, a new family of rational mapping functions is introduced which, incidentally, include the mapping functions of WENO-IM as a special case. Results of several linear advection cases are presented to demonstrate the superior performance of the new method.

2 Numerical Methods

2.1 WENO-JS scheme

Consider a one-dimensional domain $x \in [a,\ b]$ discretized into N cells of width $\Delta x = (b-a)/N$. The center and interface locations of the i^{th} cell are denoted by x_i and $x_{i\pm1/2} = x_i \pm \Delta x/2$, respectively. In the finite volume methodology, the discrete solution to a problem is determined in terms of cell averages. Given a function $u(x)$, its i^{th} cell average is denoted by $\overline{u_i}$. In this section, the left-biased fifth and seventh order WENO-JS approximations to the point value $u^L_{i+1/2} = \lim_{x\to x^-_{i+1/2}} u(x)$ is briefly outlined. The stencils for the fifth and seventh order reconstructions are shown in Figure 1.

The WENO-JS procedure begins with the computation of r^{th} order approximations to $u^L_{i+1/2}$ as shown below.

$$u^L_{i+1/2} = \left(\hat{u}^{L,r}_{i+1/2}\right)_j + O\left(\Delta x^r\right) \quad j \in [0,\ r-1] \tag{1}$$

For the fifth order WENO-JS scheme ($r = 3$), three third order approximations are obtained using the following expressions.

$$\begin{aligned}
\left(\hat{u}^{L,3}_{i+1/2}\right)_0 &= \frac{1}{6}\left(2\overline{u_{i-2}} - 7\overline{u_{i-1}} + 11\overline{u_i}\right) \\
\left(\hat{u}^{L,3}_{i+1/2}\right)_1 &= \frac{1}{6}\left(-\overline{u_{i-1}} + 5\overline{u_i} + 2\overline{u_{i+1}}\right) \\
\left(\hat{u}^{L,3}_{i+1/2}\right)_2 &= \frac{1}{6}\left(2\overline{u_i} + 5\overline{u_{i+1}} - \overline{u_{i+2}}\right)
\end{aligned} \tag{2}$$

Similarly, for the seventh order WENO-JS scheme ($r = 4$), four fourth order approximations are obtained using the following expressions.

$$\begin{aligned}
\left(\hat{u}^{L,4}_{i+1/2}\right)_0 &= \frac{1}{12}\left(-3\overline{u_{i-3}} + 13\overline{u_{i-2}} - 23\overline{u_{i-1}} + 25\overline{u_i}\right) \\
\left(\hat{u}^{L,4}_{i+1/2}\right)_1 &= \frac{1}{12}\left(\overline{u_{i-2}} - 5\overline{u_{i-1}} + 13\overline{u_i} + 3\overline{u_{i+1}}\right) \\
\left(\hat{u}^{L,4}_{i+1/2}\right)_2 &= \frac{1}{12}\left(-\overline{u_{i-1}} + 7\overline{u_i} + 7\overline{u_{i+1}} - \overline{u_{i+2}}\right) \\
\left(\hat{u}^{L,4}_{i+1/2}\right)_3 &= \frac{1}{12}\left(3\overline{u_i} + 13\overline{u_{i+1}} - 5\overline{u_{i+2}} + \overline{u_{i+3}}\right)
\end{aligned} \tag{3}$$

By performing a weighted average of these r^{th} order approximations using the optimal weights $d^{(r)}_j$, it is possible to obtain the $(2r-1)^{th}$ order upstream central approximation $u^{L,C(2r-1)}_{i+1/2}$ as shown below in Eq.(4).

$$u^{L,C(2r-1)}_{i+1/2} = \sum_{j=0}^{r-1} d^{(r)}_j \left(\hat{u}^{L,r}_{i+1/2}\right)_j \tag{4}$$

The optimal weights for fifth and seventh order WENO-JS schemes are given in Eq.(5) and Eq.(6), respectively.

$$d^{(3)}_0 = \frac{1}{10}, \quad d^{(3)}_1 = \frac{6}{10}, \quad d^{(3)}_2 = \frac{3}{10} \tag{5}$$

$$d^{(4)}_0 = \frac{1}{35}, \quad d^{(4)}_1 = \frac{12}{35}, \quad d^{(4)}_2 = \frac{18}{35}, \quad d^{(4)}_3 = \frac{4}{35} \tag{6}$$

For each r^{th} order approximation, a corresponding smoothness indicator is computed. Following [5], the r^{th} order smoothness indicator $IS^{(r)}_j$ is defined as

$$IS^{(r)}_j = \sum_{l=1}^{r-1} \Delta x^{2l-1} \int_{x_{i-1/2}}^{x_{i+1/2}} \left[\frac{d^l p_j(x)}{dx^l}\right]^2 dx \tag{7}$$

where $p_j(x)$ refers to the r^{th} order polynomial reconstructed on the j^{th} stencil which extends from cell

$(i+j-r+1)$ to cell $(i+j)$. The explicit forms of $IS_j^{(r)}$ are given below for $(r=3)$ and $(r=4)$.

$$
\begin{aligned}
IS_0^{(3)} =& \frac{1}{4}\left(\overline{u_{i-2}} - 4\overline{u_{i-1}} + 3\overline{u_i}\right)^2 + \frac{13}{12}\left(\overline{u_{i-2}} - 2\overline{u_{i-1}} + \overline{u_i}\right)^2 \\
IS_1^{(3)} =& \frac{1}{4}\left(\overline{u_{i-1}} - \overline{u_{i+1}}\right)^2 + \frac{13}{12}\left(\overline{u_{i-1}} - 2\overline{u_i} + \overline{u_{i+2}}\right)^2 \\
IS_2^{(3)} =& \frac{1}{4}\left(3\overline{u_i} - 4\overline{u_{i+1}} + \overline{u_{i+2}}\right)^2 + \frac{13}{12}\left(\overline{u_i} - 2\overline{u_{i+1}} + \overline{u_{i+2}}\right)^2
\end{aligned}
\tag{8}
$$

$$
\begin{aligned}
IS_0^{(4)} =& \left(\frac{1}{3}\overline{u_{i-3}} - \frac{3}{2}\overline{u_{i-2}} + 3\overline{u_{i-1}} - \frac{11}{6}\overline{u_i}\right)^2 + \frac{13}{12}\left(\overline{u_{i-3}} - 4\overline{u_{i-2}} + 5\overline{u_{i-1}} - 2\overline{u_i}\right)^2 \\
&+ \frac{781}{720}\left(\overline{u_{i-3}} - 3\overline{u_{i-2}} + 3\overline{u_{i-1}} - \overline{u_i}\right)^2 \\
IS_1^{(4)} =& \left(\frac{1}{6}\overline{u_{i-2}} - \overline{u_{i-1}} + \frac{1}{2}\overline{u_i} + \frac{1}{3}\overline{u_{i+1}}\right)^2 + \frac{13}{12}\left(\overline{u_{i-1}} - 2\overline{u_i} + \overline{u_{i+1}}\right)^2 \\
&+ \frac{781}{720}\left(\overline{u_{i-2}} - 3\overline{u_{i-1}} + 3\overline{u_i} - \overline{u_{i+1}}\right)^2 \\
IS_2^{(4)} =& \left(\frac{1}{3}\overline{u_{i-3}} + \frac{1}{2}\overline{u_{i-2}} - \overline{u_{i-1}} + \frac{1}{6}\overline{u_i}\right)^2 + \frac{13}{12}\left(\overline{u_{i-1}} - 2\overline{u_i} + \overline{u_{i+1}}\right)^2 \\
&+ \frac{781}{720}\left(\overline{u_{i-1}} - 3\overline{u_i} + 3\overline{u_{i+1}} - \overline{u_{i+2}}\right)^2 \\
IS_3^{(4)} =& \left(\frac{11}{6}\overline{u_i} - 3\overline{u_{i+1}} + \frac{3}{2}\overline{u_{i+2}} - \frac{1}{3}\overline{u_{i+3}}\right)^2 + \frac{13}{12}\left(2\overline{u_i} - 5\overline{u_{i+1}} + 4\overline{u_{i+2}} - \overline{u_{i+3}}\right)^2 \\
&+ \frac{781}{720}\left(\overline{u_i} - 3\overline{u_{i+1}} + 3\overline{u_{i+2}} - \overline{u_{i+3}}\right)^2
\end{aligned}
\tag{9}
$$

With the smoothness indicators computed, the non-linear WENO-JS stencil weights ω_j can be computed as follows. The superscripts (r) and $(2r-1)$ will be dropped for the sake of conciseness. The value of ϵ is taken to be 10^{-6} for WENO-JS scheme and 10^{-40} for all the mapped WENO schemes as recommended in [1].

$$
\alpha_j = \frac{d_j}{\left(IS_j + \epsilon\right)^2}, \qquad \omega_j = \frac{\alpha_j}{\sum_{j=0}^{r-1} \alpha_j}
\tag{10}
$$

Finally, the $(2r-1)^{th}$ order WENO-JS approximation $u_{i+1/2}^{L,W}$ is obtained by taking a weighted average of the r^{th} order approximations using ω_j as shown below.

$$
u_{i+1/2}^{L,W} = \sum_{j=0}^{r-1} \omega_j \left(\hat{u}_{i+1/2}^{L}\right)_j
\tag{11}
$$

2.2 Mapped WENO schemes

In order for the WENO-JS approximation in Eq.(11) to converge at the optimal $(2r-1)^{th}$ order in smooth regions, ω_j has to satisfy the following criterion.

$$
\omega_j - d_j = O\left(\Delta x^{r-1}\right)
\tag{12}
$$

A critical point is defined as a point where one or more derivatives of the function $u(x)$ vanish. At a critical point $x = x_c$ of order n_{cp}, the first n_{cp} derivatives of the function $u(x)$ vanish, i.e. $u^{'}(x_c) = \cdots = u^{(n_{cp})}(x_c) = 0$. It can be shown that the WENO-JS approximation exhibits the convergence behaviour shown in Eq.(13) [2]. When n_{cp} increases, the order of convergence deteriorates; when no derivatives vanish, i.e. $n_{cp} = 0$, WENO-JS approximation convergences at the optimal order.

$$\omega_j - d_j = O\left(\Delta x^{r-1-n_{cp}}\right) \quad \text{for} \quad n_{cp} = 1,\ \cdots,\ r-1 \tag{13}$$

Now, consider a mapping function $g(\omega)$ with the following properties:

(a) $g(0) = 0$, $g(d) = d$ and $g(1) = 1$

(b) monotone increasing with finite slopes for $\omega \in [0,\ 1]$

(c) $g^{'}(d) = \cdots = g^{(k)}(d) = 0 \neq g^{(k+1)}(d)$, i.e. the function flattens near $\omega = d$

The mapping function $g(\omega)$ can be used to calculate the mapped weights $\tilde{\omega}_j$ from the WENO-JS weights ω_j obtained from Eq.(10) as shown in Eq.(14). The mapped WENO approximation of $u^L_{i+1/2}$ is obtained by replacing ω_j in Eq.(11) with the mapped weights $\tilde{\omega}_j$.

$$\tilde{\omega}_j = \frac{g(\omega_j)}{\sum_{j=0}^{r-1} g(\omega_j)} \tag{14}$$

Following [1], the mapping function $g(\omega)$ can be expanded using Taylor series about $\omega_j = d_j$ to demonstrate that the mapping process is indeed able to recover the optimal order of accuracy near critical points.

$$g(\omega_j) = g(d_j) + \sum_{l=1}^{k} \frac{1}{l!} g^{(l)}(d_j)(\omega_j - d_j)^l + \frac{1}{(k+1)!} g^{(k+1)}(d_j)(\omega_j - d_j)^{k+1} + \cdots \tag{15}$$

Eq.(15) can be simplified using the properties of the mapping function mentioned earlier. From property (a), $g(d_j) = d_j$ and due to property (c), all the terms inside the summation vanish. Finally, substituting Eq.(13) into the result and rearranging yields the following.

$$g(\omega_j) = d_j + \frac{1}{(k+1)!} g^{(k+1)}(d_j)(\omega_j - d_j)^{k+1} + \cdots = d_j + O\left(\Delta x^{(k+1)(r-1-n_{cp})}\right) \tag{16}$$

Substituting Eq.(16) into Eq.(14) and using the fact that d_j sum to unity results in Eq.(17). Comparing this result with Eq.(12), it can be concluded that as long as $(k+1)(r-1-n_{cp}) \geq r-1$, the mapped weights $\tilde{\omega}_j$ satisfy the required criterion. For example, for fifth order convergence at a critical point of order $n_{cp} = 1$, k must be equal to or greater than 1.

$$\tilde{\omega}_j - d_j = O\left(\Delta x^{(k+1)(r-1-n_{cp})}\right) \tag{17}$$

The mapping functions from [1] and [2], denoted by g_{M} and g_{IM} respectively, are given below. In the function $g_{\mathrm{IM}}(\omega;\ k,\ A)$, k is a positive even integer and A is a positive real number. It can be shown that $g_{\mathrm{M}}(\omega) = g_{\mathrm{IM}}(\omega;\ 2,\ 1)$, i.e. g_{M} belongs to the g_{IM} family of functions. g_{IM} satisfies all the properties (a)-(c) mentioned earlier.

$$g_{\mathrm{M}}(\omega) = \frac{\omega\left(d + d^2 - 3d\omega + \omega^2\right)}{d^2 + (1-2d)\omega} \tag{18}$$

$$g_{\mathrm{IM}}(\omega;\ k,\ A) = d + \frac{A(\omega - d)^{k+1}}{(\omega - d)^k + A\omega(1-\omega)} \tag{19}$$

Feng et. al [2] found that $g_{\mathrm{IM}}(\omega;\ 2,\ 0.1)$ vastly outperformed $g_{\mathrm{M}}(\omega)$ for fifth order WENO schemes. Both the mapping functions are shown in Figure 2 for the smallest and largest values of the optimal weights d_j. Notice that $g_{\mathrm{IM}}(\omega;\ 2,\ 0.1)$ is much flatter than $g_{\mathrm{M}}(\omega)$ near $\omega_j = d_j$. As a result, $g_{\mathrm{IM}}(\omega;\ 2,\ 0.1)$ is quicker to bring the mapped weights $\tilde{\omega}_j$ close to the optimal weights d_j compared to $g_{\mathrm{M}}(\omega)$. Another important property is the slope of the mapping functions at $\omega = 0$ since this determines to some extent the level of amplification of very small weights. As evident from Eq.(20) and Figure 2, $g_{\mathrm{IM}}(\omega;\ 2,\ 0.1)$ has a much

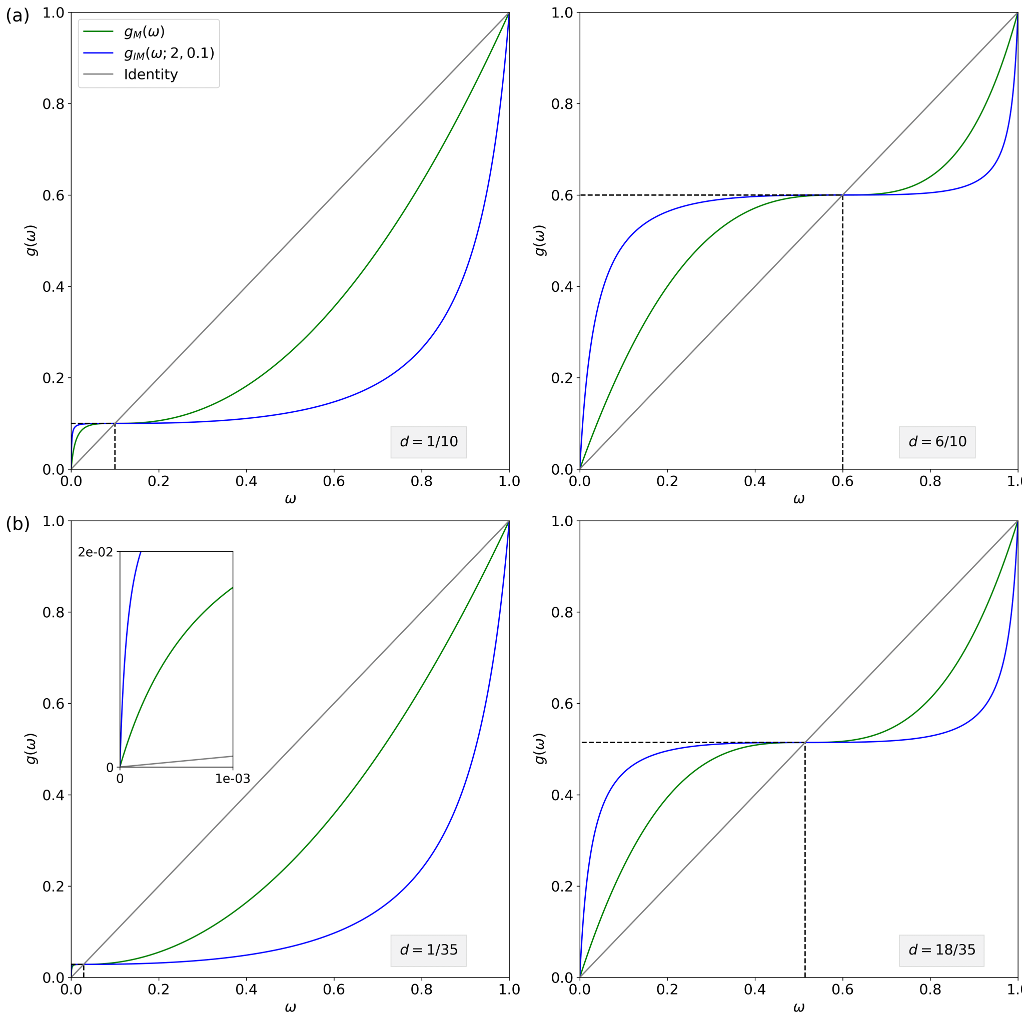

Figure 2: Mapping functions $g_{\mathrm{M}}(\omega)$ and $g_{\mathrm{IM}}(\omega;\ 2,\ 0.1)$ for the smallest and largest values of (a) $d_j^{(3)}$ and (b) $d_j^{(4)}$.

greater slope at $\omega = 0$ compared to $g_{\mathrm{M}}(\omega)$. This effect is especially pronounced at smaller values of ω. Both these properties play an important role in understanding the behaviour of the mapping process.

$$g_{\mathrm{IM}}(0;\ k,\ A) = 1 + \frac{1}{Ad^{k-1}} \tag{20}$$

2.2.1 One-dimensional linear advection

The one-dimensional linear advection problem (Eq.(21)) represents one of the most straightforward hyperbolic problems. Given the initial condition $u(x,\ t=0) = u_0(x)$, its exact solution is simply $u(x,\ t) = u_0(x-t)$ which makes it a suitable starting point for the assessment of numerical schemes. It must be remarked that the Euler equations reduce to linear advection of density in the absence of velocity and pressure gradients.

$$\partial_t u + \partial_x u = 0 \tag{21}$$

Averaging Eq.(21) over the i^{th} cell results in the ordinary differential equation for the cell average $\overline{u_i}$

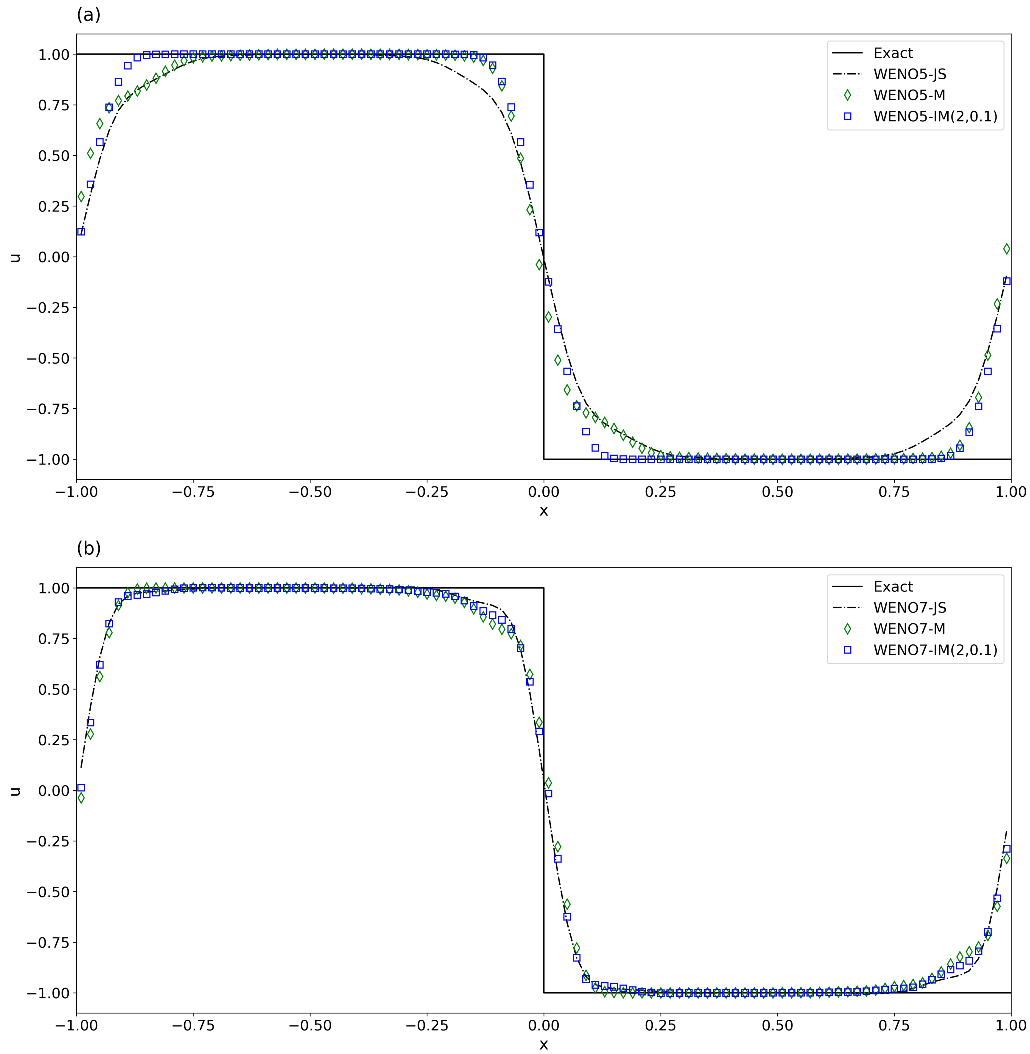

Figure 3: Performance of (a) fifth and (b) seventh order WENO schemes for linear advection of sharp discontinuity ($N = 100$ cells, $t = 200s$).

shown below. Notice that the right hand side of this equation involves the left-biased approximations of $u(x)$ at the cell interfaces which can be obtained through the WENO schemes described in the previous sections. This ODE can be solved in time using the explicit third order TVD Runge-Kutta time marching scheme.

$$\frac{d\overline{u_i}}{dt} = -\frac{1}{\Delta x}\left(u^L_{i+1/2} - u^L_{i-1/2}\right) \tag{22}$$

With the numerical schemes defined, consider the initial condition of two constant states separated by a discontinuity at $x = 0$ as shown in Eq.(23). This problem was solved on the periodic domain $x \in [-1,\ 1]$ discretized into 100 uniform cells using fifth and seventh order WENO schemes. Note that the mapped WENO methods using $g_{\mathrm{M}}(\omega)$ and $g_{\mathrm{IM}}(\omega;\ 2,\ 0.1)$ are denoted by WENO-M and WENO-IM(2,0.1), respectively. The results are shown in Figure 3 at $t = 200s$ (100 cycles) with CFL=0.1.

$$u_0(x) = \begin{cases} +1, & -1 \leq x \leq 0 \\ -1, & 0 < x \leq 1 \end{cases} \tag{23}$$

It can be observed from Figure 3(a) that at fifth order the mapped WENO schemes WENO-M and WENO-IM(2,0.1) are able to capture the discontinuities with lesser numerical diffusion compared to WENO-JS scheme. Between the mapped WENO schemes, WENO-IM(2,0.1) is superior as it is able to capture the flat regions on both sides of the discontinuities accurately. In contrast, WENO-M suffers a loss of accuracy to the right (upstream) of the discontinuities and performs similar to WENO-JS scheme. The situation is quite different at seventh order as seen from Figure 3(b). Both the mapped WENO schemes deliver a similar, and at some regions even worse, performance compared to WENO-JS scheme. WENO-IM(2,0.1) suffers a particularly significant loss in accuracy at the flat regions slightly to the left (downstream) of the discontinuities.

To understand the reason behind this loss in accuracy, the mapped weights were analysed in detail. The mapped weights $\tilde{\omega}_{r-1}$ for the rightmost stencil are plotted for the fifth and seventh order WENO-IM(2,0.1) schemes in Figure 4 at the end of the first cycle ($t = 2s$). First of all, it must be noted that $\tilde{\omega}_{r-1} \approx d_{r-1}$ in the middle of the discontinuity itself for both fifth and seventh orders because it has been sufficiently "smoothened" by numerical diffusion. The areas of concern are actually the regions slightly adjacent to the smeared discontinuity before the profile becomes completely flat where once again $\tilde{\omega}_{r-1} \approx d_{r-1}$. It can be seen from Figure 4(a) that for the fifth order, $\tilde{\omega}_2 \approx 1$ to the right and very small to the left. This is the expected behaviour since the solution becomes less smooth as one moves from the flat regions towards the discontinuity. For the seventh order, the weights to the right behave in the appropriate manner. However, at some points to the left of the discontinuity (see shaded region in Figure 4(b)), $\tilde{\omega}_3$ do not drop to small values like their neighbours. Since this is the most prominent difference between the behaviours of $\tilde{\omega}_{r-1}$ at fifth and seventh orders, it is believed to be the reason behind the poor performance of WENO-IM(2,0.1) at seventh order. This claim is supported by the results shown in Figure 3(b) whereby the loss of accuracy occurs precisely around the affected region. In fact, this trend was observed in other test cases as well.

Upon closer examination of the smoothness indicators IS_j at the affected points, it was revealed that the smoothness indicator of the smoothest stencil ($j = 0$) was only one to two orders of magnitude smaller than the smoothness indicator of the least smooth stencil ($j = 3$), i.e. $IS_0/IS_3 = O\left(10^{-2}\right)$. In contrast, at the neighbouring points with smaller values of $\tilde{\omega}_3$, they were between four to five orders of magnitude apart. In the affected region, the unmapped WENO-JS weights ω_3 are approximately $O\left(10^{-4}\right)$ but when they undergo mapping by $g_{\mathrm{IM}}\left(\omega;\ 2,\ 0.1\right)$, they become amplified by nearly two orders of magnitude such that $\tilde{\omega}_3 = O\left(10^{-2}\right)$. This amplification is attributed to the large slope of $g_{\mathrm{IM}}\left(\omega;\ 2,\ 0.1\right)$ at $\omega = 0$ especially for small values of d_j. It is apparent from the results that this amplification is detrimental to accuracy at seventh order.

2.2.2 A new family of mapping functions

Based on the discussion in the previous section, it appears that limiting the amplification of small weights is important for seventh order mapped WENO schemes. With this idea in mind, consider a more general family of *r*ational *m*apping functions g_{RM}. In g_{RM}, k is a positive even integer, m a positive integer and s a positive scaling factor. g_{RM} includes g_{IM} as a special case for $m = 1$ and $s = A^{-1}$.

$$g_{\mathrm{RM}}\left(\omega;\ k,\ m,\ s\right) = d + \frac{\left(\omega - d\right)^{k+1}}{\left(\omega - d\right)^{k} + s\left[\omega\left(1-\omega\right)\right]^{m}} \tag{24}$$

The distinguishing feature of g_{RM} is that for $m > 1$, $g'_{\mathrm{RM}}\left(0;\ k,\ m,\ s\right) = 1$. As evident from Figure 5, g_{RM} functions follows the identity map $g\left(\omega\right) = \omega$ close to $\omega = 0$. This means that small weights are preserved with little or no amplification upon mapping with g_{RM} functions. Increasing the value of m causes the mapping function to move closer to the identity map which provides an additional degree of control over the mapping process. Therefore, for $m > 1$, g_{RM} could be more suitable for mapped WENO schemes at seventh order and above.

It is crucial that g_{RM} satisfies all the three properties (a)-(c) mentioned earlier. It can be easily verified that g_{RM} satisfies properties (a) and (c). However, it does not satisfy property (b) unconditionally. g_{RM} can be non-monotone and determining the exact conditions for monotonicity is not very straightforward. Nevertheless, monotonicity can be easily proven for specific combinations of k and m. For instance, the monotonicity of $g_{\mathrm{RM}}\left(\omega;\ 4,\ 4,\ s\right)$ can be proven as described next.

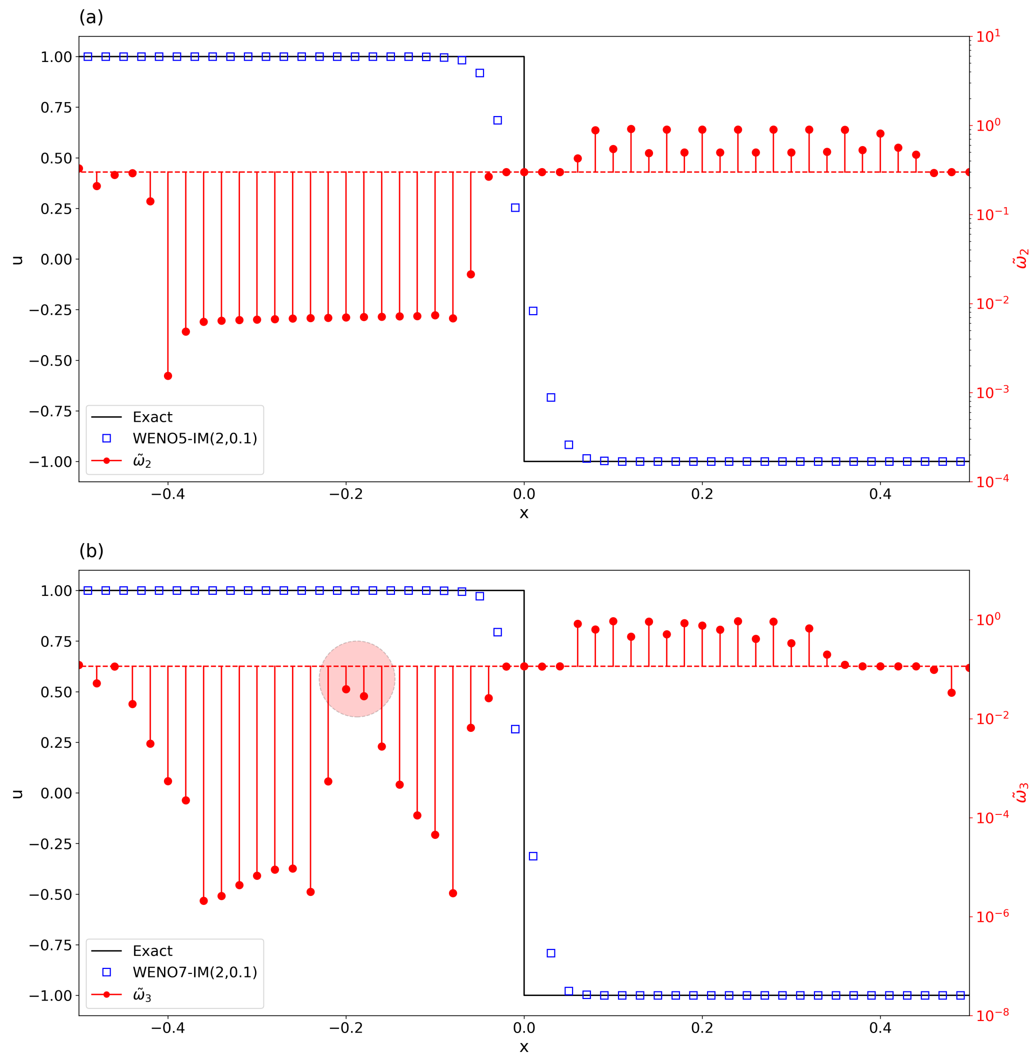

Figure 4: Mapped weights of rightmost stencil $\tilde{\omega}_{r-1}$ for (a) fifth and (b) seventh order WENO-IM(2,0.1) scheme at the end of first cycle ($t = 2s$). The optimal weights d_{r-1} are indicated by the dotted red line.

The first derivative of $g_{\mathrm{RM}}(\omega;\ 4,\ 4,\ s)$ is given below. To prove the monotonicity of $g_{\mathrm{RM}}(\omega;\ 4,\ 4,\ s)$, it is sufficient to prove the positivity of the quadratic term $h(\omega) = 3\omega^2 + (1-8d)\omega + 4d$ which appears in the numerator since all the remaining terms are greater than or equal to 0.

$$g_{\mathrm{RM}}^{'}(\omega;\ 4,\ 4,\ s) = \frac{(\omega-d)^4 \left\{ (\omega-d)^4 + s\left[\omega(1-\omega)\right]^3 \overbrace{\left[3\omega^2 + (1-8d)\omega + 4d\right]}^{h(\omega)} \right\}}{\left\{ (\omega-d)^4 + s\left[\omega(1-\omega)\right]^4 \right\}^2} \tag{25}$$

$h(\omega)$ passes through the points $(0, 4d)$ and $(1, 4(1-d))$. Had the coefficient of ω^2 in $h(\omega)$ been negative, this would have been sufficient to prove the positivity of $h(\omega)$ since $h(\omega) \geq \min\left[4d,\ 4(1-d)\right] > 0$ in the interval $\omega \in [0,\ 1]$. In this case, however, since the coefficient of ω^2 is positive, it is necessary to check the location of the minimum point. $h(\omega)$ has a minimum point which occurs at $\omega_{\min} = (8d-1)/6$ and $h(\omega_{\min}) = 4d - (1-8d)^2/12$. Table 1 shows the values of $\omega_{\min}$ and, if $0 \leq \omega_{\min} \leq 1$, the corresponding

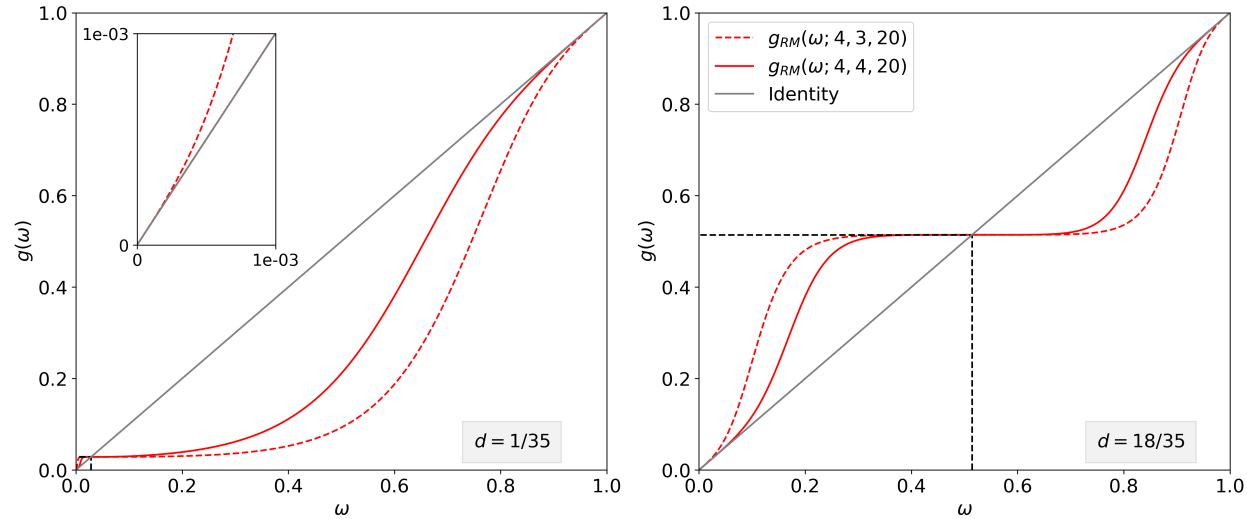

Figure 5: g_{RM} mapping functions for different values of m for the smallest and largest values of $d_j^{(4)}$. The identity map $g(\omega) = \omega$ is shown in grey.

Table 1: Values of $\omega_{\min}$ and $h(\omega_{\min})$ for $k = m = 4$ for seventh order WENO schemes

j	d_j	$\omega_{\min}$	$h(\omega_{\min})$
0	1/35	-9/70	-
1	12/35	61/210	16439/14700
2	18/35	109/210	18359/14700
3	4/35	-1/70	-

values of $h(\omega_{\min})$ for each d_j. For $j = 0$ and $j = 3$, since the minimum point occurs beyond the interval $\omega \in [0,\ 1]$, $h(\omega) \geq \min[4d,\ 4(1-d)] > 0$. For $j = 1$ and $j = 2$, the minimum points occur within the interval $\omega \in [0,\ 1]$ but $h(\omega_{\min}) \geq 0$. Hence, $h(\omega) \geq 0$ for all d_j in the interval $\omega \in [0,\ 1]$. This proves the positivity of $g'_{\mathrm{RM}}(\omega;\ 4,\ 4,\ s)$ and, therefore, the monotonicity of $g_{\mathrm{RM}}(\omega;\ 4,\ 4,\ s)$.

After extensive numerical tests, it was determined that $g_{\mathrm{RM}}(\omega;\ 4,\ 4,\ 20)$ performed well at seventh order for a number of cases. This new mapped method will be referred to as WENO-RM(4,4,20). It must be remarked that WENO-IM(2,0.1) outperformed the best fifth order WENO-RM scheme WENO-RM(2,4,40).

The results for the sharp discontinuity case at $t = 2s$ (1 cycle) and $t = 200s$ (100 cycles) are shown in Figure 6. Notice that the mapped weights of the rightmost stencil $\tilde{\omega}_3$ remain uniformly small in the region slightly to the left of the smeared discontinuity and the discontinuity is captured accurately until the end of 100 cycles. The performance of WENO-RM(4,4,20) is compared with other seventh order WENO schemes for more cases in the next section.

3 Results

3.1 Case 1

The initial condition for case 1 (Eq.(26)) was obtained from [6]. It consists of discontinuities in u_0 at $x = 7/8$, in u_0' at $x = 1/2$ and in u_0'' at $x = 1/8$. It also possesses a smooth maximum at $x = 3/8$. It was solved on the periodic domain $x \in [0,\ 1]$ discretized uniformly into $N = 50$, 100 and 200 cells until $t = 100s$ (100

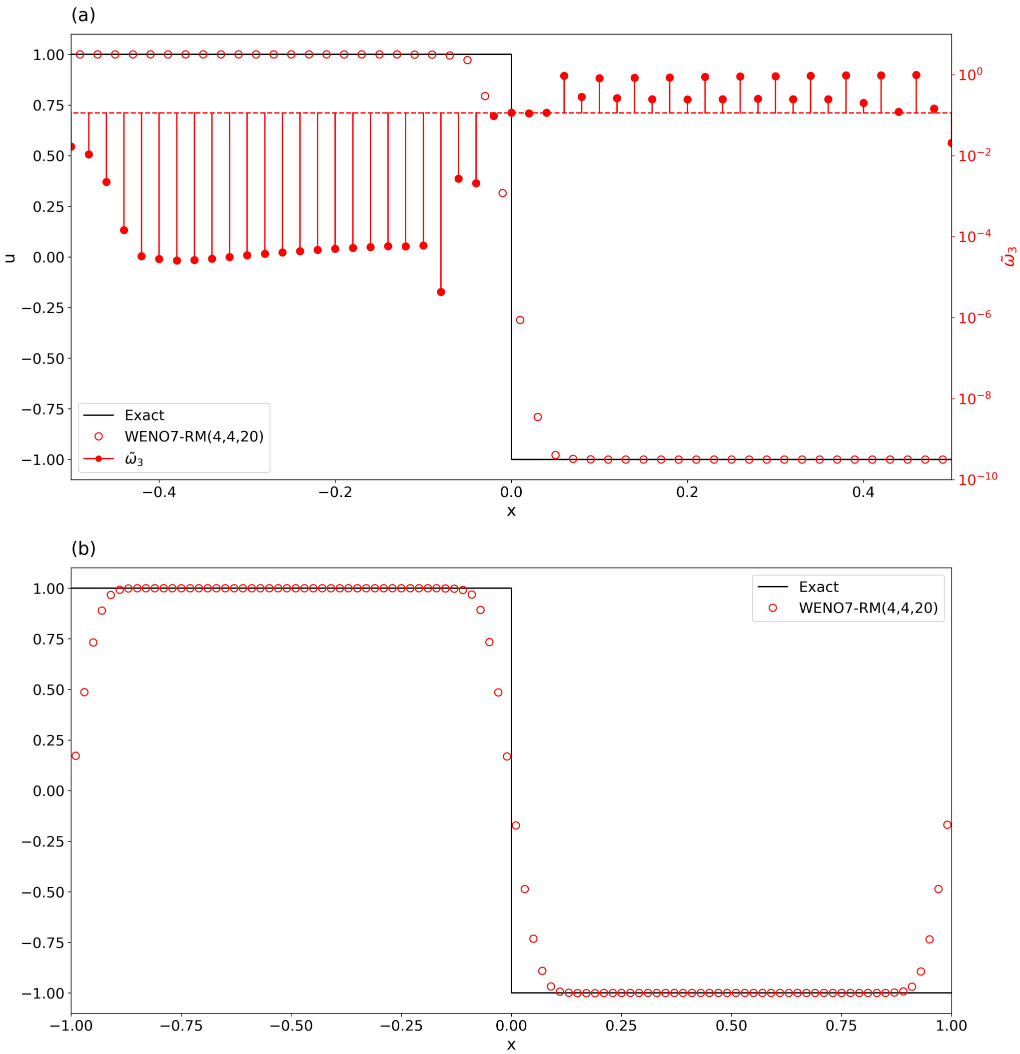

Figure 6: (a) Mapped weights of rightmost stencil $\tilde{\omega}_3$ for seventh order WENO-RM(4,4,20) scheme at $t = 2s$, (b) Performance of seventh order WENO-RM(4,4,20) scheme for linear advection of sharp discontinuity at $t = 200s$.

cycles) with CFL=0.1.

$$u_0(x) = \begin{cases} 0, & x \leq 1/8 \text{ or } x \geq 7/8 \\ [1 - \sin(4\pi x)]/2, & 1/8 < x \leq 1/2 \\ 1/2, & 1/2 < x \leq 7/8 \end{cases} \tag{26}$$

The L_1 error norms and convergence rates are listed in Table 2. WENO-RM(4,4,20) results in the smallest error at all three resolutions. At $N = 50$ cells, the mapped WENO schemes WENO-M and WENO-IM(2,0.1) perform better than WENO-JS but at $N = 200$ cells, WENO-JS surpasses them both.

The results for $N = 100$ cells are shown in Figure 7. First of all, it can be noticed that WENO-JS scheme causes flattening of the smooth maximum near $x = 0.4$. However, all three mapped WENO schemes are able to capture it accurately because they are designed to recover optimal accuracy at critical points. Secondly, WENO-RM(4,4,20) performs the best at the discontinuity at $x = 0.875$ for reasons described in the previous section. Lastly, the results near $x = 0.125$ show that both WENO-M and WENO-IM(2,0.1) start to deviate from the initial condition even though the profile is smooth in that region while WENO-RM(4,4,20) follows

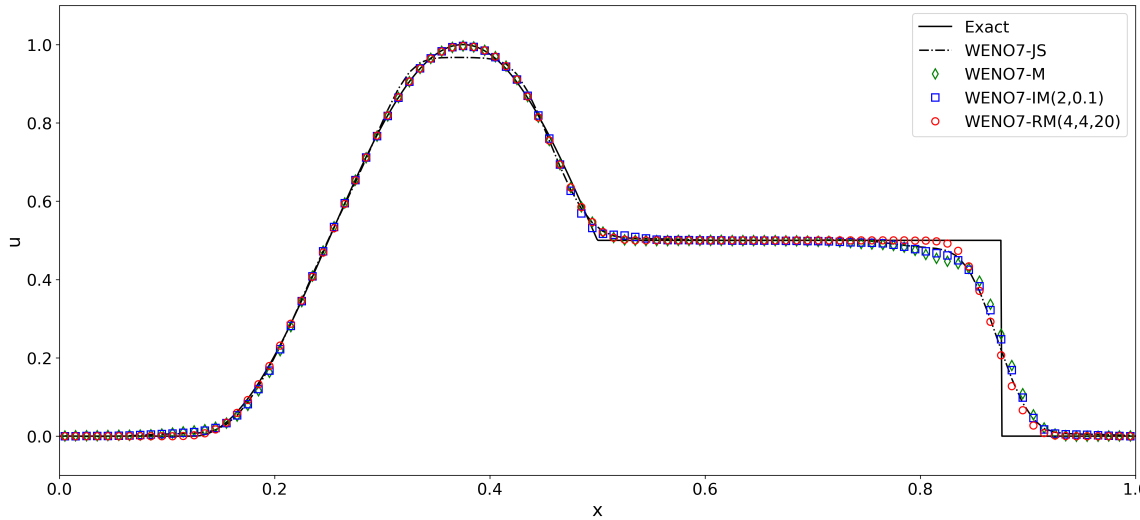

Figure 7: Performance of seventh order WENO schemes for linear advection case 1 ($N = 100$ cells, $t = 100s$).

Table 2: L_1 error norms and convergence rates (in brackets) for Case 1 at $t = 100s$

N	WENO-JS	WENO-M	WENO-IM(2,0.1)	WENO-RM(4,4,20)
50	5.9535-02	4.5550E-02	3.8432E-02	2.3875E-02
100	1.6389E-02 (1.8610)	1.5922E-02 (1.5164)	1.5247E-02 (1.3378)	1.0500E-02 (1.1851)
200	7.7120E-03 (1.0876)	1.0101E-02 (0.6565)	9.5012E-03 (0.6823)	5.2943E-03 (0.9879)

the initial profile well. This suggests that WENO-IM(2,0.1) and WENO-M may suffer from a similar loss of accuracy even when initial profile is smooth. After all, the initial profile in this region resembles a smeared discontinuity.

3.2 Case 2

The initial condition for case 2 (Eq.(27)) was obtained from [5]. From left to right, it consists of four profiles: a combinations of Gaussians, a square wave, a triangle wave and a half-ellipse. It was solved on the periodic domain $x \in [-1,\ 1]$ discretized uniformly into $N = 200$, 400 and 800 cells until $t = 200s$ (100 cycles) with CFL=0.1.

$$u_0(x) = \begin{cases} \frac{1}{6}\left[G(x,-\delta) + G(x,+\delta) + 4G(x,0)\right], & -0.8 \le x \le -0.6 \\ 1, & -0.4 < x \le -0.2 \\ 1 - 10|x - 0.1|, & 0 \le x \le 0.2 \\ \frac{1}{6}\left[F(x,-\delta) + F(x,+\delta) + 4F(x,0)\right], & 0.4 \le x \le 0.6 \\ 0, & \text{otherwise} \end{cases} \tag{27}$$

where $G(x,z) = \exp\left[-\beta(x + 0.7 + z)^2\right]$, $F(x,z)\sqrt{\max\left[0,\ 1 - 100(x - 0.5 + z)^2\right]}$, $\beta = \log 2/36\delta^2$ and $\delta = 0.005$.

The L_1 error norms and convergence rates are listed in Table 3. Once again, WENO-RM(4,4,20) produces the smallest error at all three resolutions. For this case, WENO-JS performs worse than WENO-IM(2,0.1) consistently.

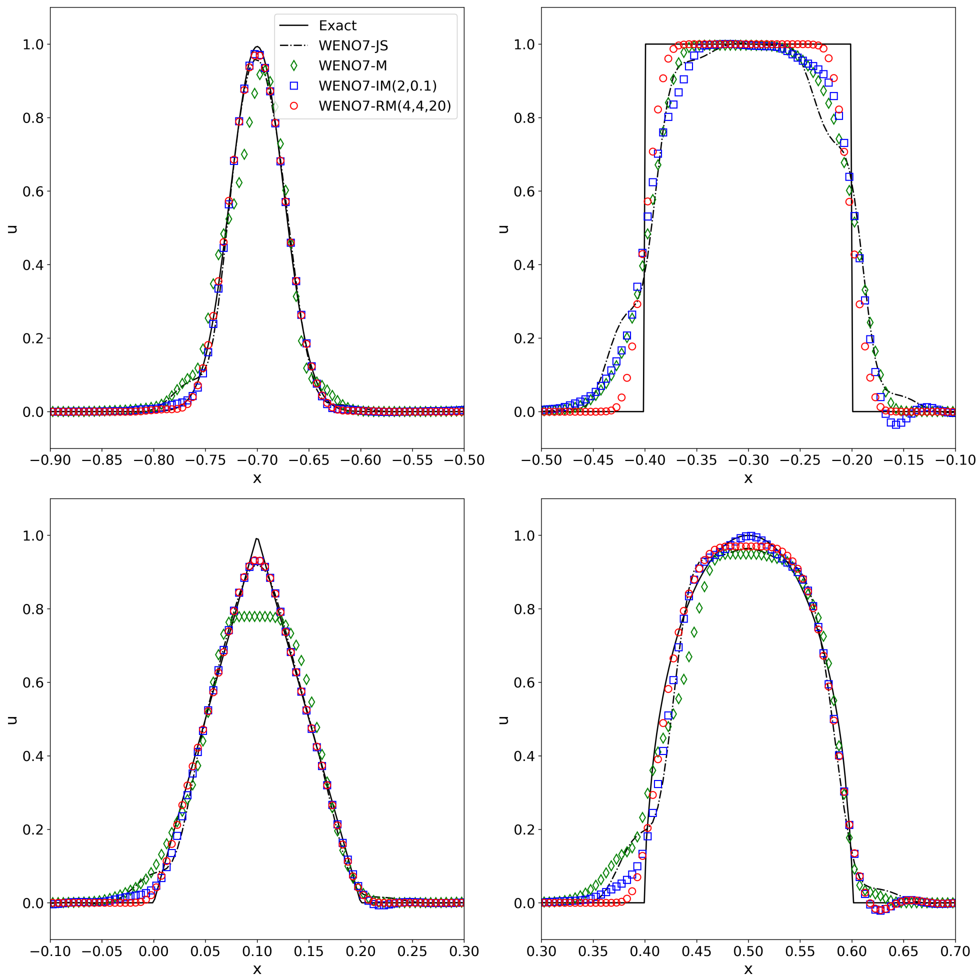

Figure 8: Performance of seventh order WENO schemes for linear advection case 2 ($N = 400$ cells, $t = 200s$).

Table 3: L_1 error norms and convergence rates (in brackets) for Case 2 at $t = 100s$

N	WENO-JS	WENO-M	WENO-IM(2,0.1)	WENO-RM(4,4,20)
200	6.5253E-02	8.8073E-02	5.8925E-02	3.6474E-02
400	3.7072E-02 (0.8157)	4.0109E-02 (1.0118)	2.7353E-02 (1.1072)	1.6788E-02 (1.1194)
800	2.0599E-02 (0.8478)	1.9150E-02 (1.0666)	1.1360E-02 (1.2678)	8.3430E-03 (1.0088)

The results for $N = 400$ cells are shown in Figure 8. Each individual profile is shown separately for clarity. It is evident that WENO-RM(4,4,20) provides the best overall performance for this case. First of all, with the exception of a single spurious oscillation near $x = 0.625$, WENO-RM(4,4,20) captures the sharp transitions of all profiles accurately. All other schemes result in noticeable dissipation on either sides of the square wave. WENO-JS and WENO-M also result in severe degradation along the left side of the semi-ellipse. Secondly, WENO-RM(4,4,20) captures the highest peaks for the Gaussian profile and triangle wave. WENO-M, however, results in a skewed Gaussian profile and considerably flattened peaks for the triangle wave and semi-ellipse. Interestingly, only WENO-IM(2,0.1) is able to capture the peak of the semi-ellipse with little flattening. It was found that WENO-IM(2,0.1) assigned (nearly) optimal weights at the peak.

The extent of flattening by the other schemes reflects how far the mapped weights were from the optimal weights.

4 Conclusion and Future Work

In this study, the performance of the seventh order mapped scheme WENO-IM(2,0.1) was analyzed in detail. The mapping process using $g_{\mathrm{IM}}(\omega;\ 2,\ 0.1)$ tends to amplify very small weights. While this is tolerable and may even be beneficial to its success at fifth order, the amplification was found to be excessive at seventh order which resulted in its poor performance. The reason for this over-amplification is the large slope of $g_{\mathrm{IM}}(\omega;\ 2,\ 0.1)$ at $\omega = 0$ which is in turn due to the smaller numerical values of d_j at seventh order. Therefore, it is believed that this problem will worsen at higher orders due to the even smaller values of d_j. A simple solution was suggested in the form of a more general family of mapping functions $g_{\mathrm{RM}}(\omega;\ k,\ m,\ s)$. For $m > 1$, these mapping functions have unit slope at $\omega = 0$ regardless of the values of d_j. This would prevent the over-amplification of small weights making it particularly suitable at seventh order and above. It was shown through several linear advection test cases that WENO-RM(4,4,20) performed significantly better compared to WENO-IM(2,0.1) and WENO-M.

Despite its success, there are still a number of areas to improve upon. For instance, as seen from the results of linear advection case 2, WENO-RM(4,4,20) produces spurious oscillations at the foot of some profiles and flattens the peak of the semi-ellipse. The remedies for these two problems impose contradicting requirements on the mapping function since eliminating spurious oscillations requires further attenuation of the weights of non-smooth stencils while capturing a smooth profile accurately requires the mapped weights to reach their optimal values quicker. Therefore, it appears that a single mapping function may not be suitable under all circumstances. Numerical studies are under way to develop a new mapping method based on this insight.

Acknowledgements

The authors gratefully acknowledge the support for the present work by Singapore Ministry of Education AcRF Tier-2 grant (MOE2014-T2-1-002), National Supercomputing Center Singapore (NSCC) and support for the first author through Graduate Research Officer scholarship from School of Mechanical and Aerospace Engineering, Nanyang Technological University, Singapore.

References

[1] A. K. Henrick, T. D. Aslam, and J. M. Powers. Mapped weighted essentially non-oscillatory schemes: Achieving optimal order near critical points. *Journal of Computational Physics*, 207(2):542–567, 2005.

[2] H. Feng, C. Huang, and R. Wang. An improved mapped weighted essentially non-oscillatory scheme. *Applied Mathematics and Computation*, 232(Supplement C):453–468, 2014.

[3] A. Harten, B. Engquist, S. Osher, and S. R. Chakravarthy. Uniformly high order accurate essentially non-oscillatory schemes, iii. *Journal of Computational Physics*, 71(2):231–303, 1987.

[4] X. D. Liu, S. Osher, and T. Chan. Weighted essentially non-oscillatory schemes. *Journal of Computational Physics*, 115(1):200–212, 1994.

[5] G. S. Jiang and C. W. Shu. Efficient implementation of weighted eno schemes. *Journal of Computational Physics*, 126(1):202–228, 1996.

[6] P. N. Blossey and D. R. Durran. Selective monotonicity preservation in scalar advection. *Journal of Computational Physics*, 227(10):5160–5183, 2008.